International Journal of Thermophysics, Vol. 9, No. 5, 1988

Heat Transfer in Thermal Insulations—Recent Progress in Analysis[1]

J. Fricke[2] and R. Caps[2]

Thermal insulations made of fibers, powders, or porous gels are characterized best with respect to their infrared optical thickness. (i) In optically thick insulations, where diffusion of infrared radiation occurs, the contributions from solid conduction and radiative transport are superimposed additively. (ii) For optically thin insulations a complex coupling mechanism causes the total heat transfer to be larger than the sum of the components; this holds especially for low emissivity boundaries. In this paper recent progress in the investigation of evacuated thermal insulations is reviewed.

KEY WORDS: diffusion of radiation; insulations (thermal); insulations (optically thin); radiative heat transport.

1. INTRODUCTION

Considerable efforts have been made to investigate and to reduce thermal transport in porous insulations consisting of fibers, powders, or porous gels. A collection of important results was published roughly 20 years ago by Kaganer [1]. In recent research programs the optimization of thermal resistance has been a major goal [2]. A detailed understanding of infrared (IR) radiative transport, of solid conduction and of gaseous thermal conduction, and of the mutual interaction between these heat transfer channels is a prerequisite for systematic improvements. Studies on this subject have included optically thick loaded fibrous insulations [3, 4] and prepressed boards of opacified fumed silica [5], as well as optically thin insulations, for example, translucent silica aerogels [6] and low-density fiber mats [7].

[1] Paper presented at the Tenth Symposium on Thermophysical Properties, June 20–23, 1988, Gaithersburg, Maryland, U.S.A.

[2] Physikalisches Institut der Universität, Am Hubland, D-8700 Würzburg, Federal Republic of Germany.

0195-928X/88/0900-0885$06.00/0

2. THERMAL TRANSPORT IN OPTICALLY THICK INSULATIONS

2.1. The Total Conductivity and Its Components

The total conductivity λ as a function of external load p_{ext}, temperature T, or internal gas pressure p_g can be derived from calorimetric measurements using a suitable hot-plate system [8]. For evacuated specimens the conductivity λ can be split into its components, the radiative conductivity λ_r and the solid conductivity λ_{sc}, which are additively superimposed in optically thick insulations, where the diffusion approximation holds:

$$\lambda(T) = \lambda_{sc}(T) + \lambda_r(T)$$
$$\lambda_r(T) = \frac{16n^2\sigma T^3}{3E(T)} \tag{1}$$

Here n is the average index of refraction of the porous system and E is the extinction coefficient. From the caloric measurements often a dependence $\lambda(T_r) = A + BT_r^3$ results, with $T_r = [(T_1 + T_2)(T_1^2 + T_2^2)/4]^{1/3}$ being a mean radiative temperature, averaged over the specimen. The extrapolation of $\lambda(T_r)$ toward $T_r = 0$ in a λ versus T_r^3 plot produces reliable results only if λ_{sc} and E are independent of T. In other cases additional information on the IR radiative transport has to be extracted from IR extinction measurements using a FTIR spectrometer [9]. Another approach is to start from the complex index of refraction in the IR and to calculate the extinction coefficient along the lines of Mie scattering theory [9].

The results of a recent investigation of ground diatomite powder [10] demonstrate how to proceed. The total thermal conductivity λ of evacuated diatomite was measured in a typical hot-plate system [11]. A temperature dependence $\lambda \propto T_r^{\alpha}$ is observed, with α being somewhat smaller than 3 (Fig. 1). In order to extract the solid conductive and the radiative contributions the following procedure is employed.

(i) The solid conduction of diatomite λ_{sc} is assumed to be proportional to the solid conduction of massive, nonporous amorphous silica λ_0 [12], with both conductivities having the same dependence on the absolute temperature T:

$$\lambda_{sc}(T) = C_1 \cdot \lambda_0(T) \tag{2}$$

In a zeroth-order approach the constant C_1 can be determined from a comparison of λ and λ_0 at below-ambient temperatures. At 250 K the radiative contribution to the total conduction is estimated to be only a few percent.

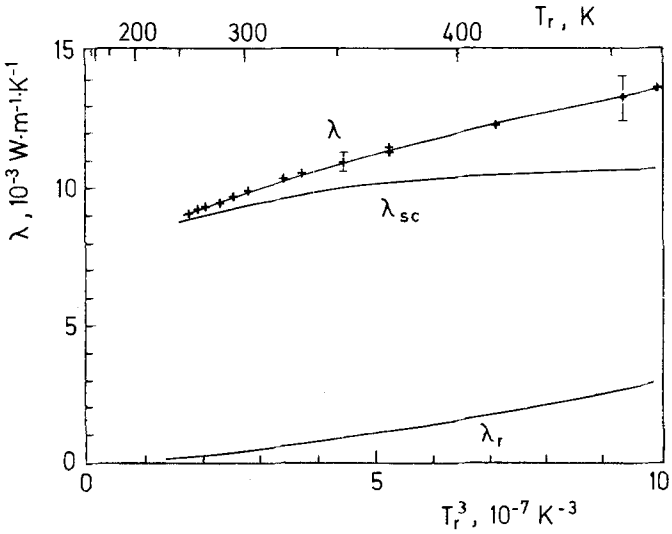

Fig. 1. Dependence of the total thermal conductivity λ of evacuated diatomite powder on the cube of the mean temperature T_r. The density of the specimen was $\rho \approx 345\,\mathrm{kg \cdot m^{-3}}$ and the external pressure load $p_{ext} = 1$ bar. Also the contributions from radiative and conductive transport, λ_r and λ_{sc}, respectively, are shown.

Thus

$$C_1 = \frac{\lambda_{sc}(250\,\mathrm{K})}{\lambda_0(250\,\mathrm{K})} = \frac{8.7 \times 10^{-3}}{1.28} = 6.8 \times 10^{-3} \tag{3}$$

It should be pointed out that it is not correct to determine C_1 merely from the density ratio of diatomite powder and fully dense silica. This ratio would be $345/2200 = 0.16$, i.e., much too large.

(ii) Subtraction of $\lambda_{sc}(T_r) = 6.8 \times 10^{-3}\,\lambda_0(T_r)$ from $\lambda(T_r)$ then allows for deduction of $\lambda_r(T_r)$ (Fig. 1). In order to check the correctness of this procedure, $\lambda_r(T_r)$ was also derived from IR optical extinction measurements and use of Eq. (1). The index of refraction of the powder is determined as follows:

$$n = 1 + (\rho/\rho_0)(n_{SiO_2} - 1) \tag{4}$$

with $n_{SiO_2} = 1.4$ for nonporous SiO_2 glass. The specific extinction coefficient

$$e = E/\rho \tag{5}$$

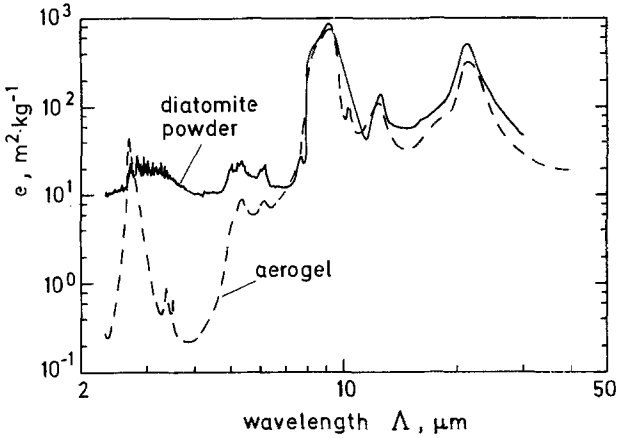

Fig. 2. Effective specific extinction $e = E/\rho$ as a function of wavelength Λ for compressed diatomite powder and nonscattering SiO_2 aerogel [10].

is determined from IR transmission measurements. The wavelength dependence of e is depicted in Fig. 2. Above 8 μm strong absorption bands, which are typical for SiO_2, occur. Below this wavelength scattering is observed. This can be seen from a comparison with extinction data of SiO_2–aerogel (Fig. 2), where the largest structures are of the order of 50 nm and therefore scattering in the IR is negligible [13].

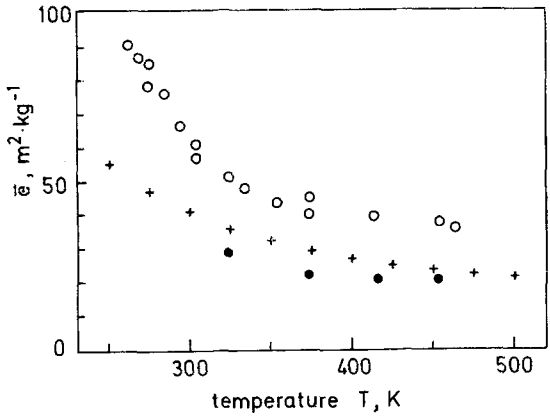

Fig. 3. Averaged effective specific extinction coefficient $\bar{e}$ as a function of temperature T for compressed diatomite tablets from IR data (+) as well as for diatomite powder from caloric measurements, with $p_{ext} = 1$ bar (○) and $p_{ext} = 5$ bar (●).

The extinction coefficient $e(\Lambda)$ has to be averaged over the diffusing thermal spectrum. The derived Rosseland mean $\bar{e}(T)$ is shown in Fig. 3. The decrease in $\bar{e}$ with T is considerable, thus λ_r is expected to increase more strongly than proportional to the third power of T. The concave curvature of λ_r indeed can be recognized in Fig. 1.

Due to the strong compression of the diatomite powder into a tablet, the character of the scattering might have changed from independent into dependent scattering [14]. In the latter case clusters of diatomite particles instead of separate grains act as scatterers for the thermal radiation. As a consequence the specific extinction coefficient for the tablets is expected to be smaller than for low-density fills. This effect can be seen precisely from Fig. 3, where $\bar{e}$ from the tablets is lower than $\bar{e}$ derived from the caloric measurements at $p_{ext} = 1$ bar.

2.2. The Variation of the Solid Conduction with the External Pressure Load

Upon compression load-bearing fiber or powder insulations generally show a marked variation of their solid conduction. This is to be expected, as with increasing pressure load, first, the thermal resistance between touching fibers or grains decreases, and second, the number of contacts grows.

In order to suppress the radiative heat transfer in the caloric measurements, the temperature ought to be chosen as low as possible ($T_r \approx 270$ to 280 K). Radiative contributions to the total conduction generally amount to a few percent under these conditions. The dependence of λ_{sc} on p_{ext} is shown in Fig. 4 for the diatomite powder and for a layer of glass-fiber papers [15]. It is obvious that the latter shows a much smaller solid conductivity. The difference in the conductivities can be understood—at least qualitatively—in terms of the phonon diffusion model [4]. According to this model the solid conduction is proportional to the density ρ and the sound velocity v of the insulation system. Thus one would expect

$$\left(\frac{\lambda_{sc}}{\rho v}\right)_{powder} = \left(\frac{\lambda_{sc}}{\rho v}\right)_{fiber} \tag{6}$$

At $p_{ext} \approx 1$ bar the fiber paper system has a density $\rho \approx 250\ \mathrm{kg \cdot m^{-3}}$ and a longitudinal sound velocity $v \approx 110\ \mathrm{m \cdot s^{-1}}$, while for the powder layer $\rho \approx 400\ \mathrm{kg \cdot m^{-3}}$ and $v \approx 300\ \mathrm{m \cdot s^{-1}}$ are determined. Thus Eq. (6) is valid within a factor of 2 or so.

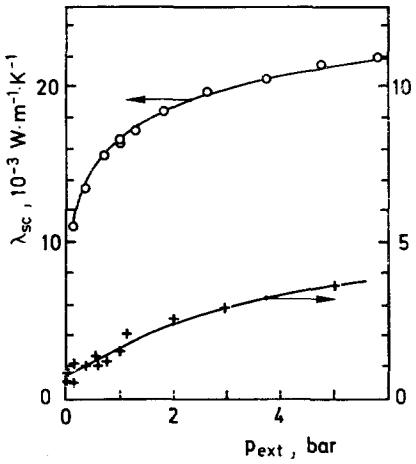

Fig. 4. Measured solid conductivity λ_{sc} upon change of external pressure load p_{ext}: (○) diatomite powder; (+) glass-fiber paper.

3. OPTICALLY THIN INSULATIONS

Here infrared photons in certain wavelength regions may penetrate the insulation without multiple scattering or absorption. The boundaries then communicate radiatively with each other in a very direct way [16, 17].

3.1. Low-Density Organic Fiber Mat

The optical thickness $\tau_0 = ED$ of a $d = 40$-mm-thick organic fiber mat with a density of $8\ \mathrm{kg \cdot m^{-3}}$ is of the order of 4. In this case the radiative heat transfer cannot be considered as a conduction process, which depends only on the local temperature gradient. The radiative flux q_r at a given point is also influenced by the emitted and scattered intensities further off this point and by the boundaries. The most convenient way to solve this problem is to use an approximate representation of the combined conduction–radiation transfer problem (see also Ref. 18). This is accomplished by starting from a three-flux representation of the equation of transfer for isotropic scattering proposed by Kaganer (cosine directions μ_{-1}, μ_0, and μ_1 and weight factors a_{-1}, a_0, and a_1) [19], which includes the 90° sideward direction ($\mu_0 = \cos 90° = 0$). The equations for the three intensities I_i ($i = -1, 0, 1$) are reduced to two differential equations plus an equation for the conservation of total flux. Assuming small temperature differences

$T_1 - T_2$ it is possible to linearize the emission term $\sigma T^4/\pi$ to $(\sigma T_r^4/\pi) \cdot (4\theta - 3)$. The intensities I_i are expressed in units of $\sigma \cdot T_r^4/\pi$:

$$\mu_i \frac{dI_i}{d\tau} = -I_i + \frac{\omega_0}{2} \sum_{i=-1}^{+1} a_i I_i + 4\theta(1-\omega_0)$$
$$N_r \frac{d^2\theta}{d\tau^2} = -(1-\omega_0)\left(\frac{1}{2}\sum_{i=1}^{+1} a_i I_i - 4\theta\right) \tag{7}$$

where $N_r = \lambda_{SG} E/4\sigma n^2 T_r^3$ is the conduction–radiation parameter, τ is the optical depth, ω is the albedo, $\theta = T/T_r$, $\mu_1 = -\mu_{-1} = \frac{2}{3}$, $a_1 = a_{-1} = \frac{3}{4}$, and $a_0 = \frac{1}{2}$.

After solving this system of linear differential equations and applying appropriate boundary conditions (emissivity of the sidewalls $\varepsilon_1 = \varepsilon_2 = \varepsilon$), the following expression for the total heat flux q or the thermal loss coefficient k is obtained:

$$k = \frac{q}{T_1 - T_2} = \frac{\lambda_\infty/d}{4/3\{N_r(p\tau_0/2)\coth(p\tau_0/2) + [\varepsilon\tau_0/(2-\varepsilon)][\frac{3}{4}N_r + 1)\}^{-1} + 1} \tag{8}$$

with

$$p = \frac{3}{2}\left[\frac{1-\omega_0}{1-\omega_0/4}\left(1 + \frac{4}{3N_r}\right)\right]^{1/2}$$

and

$$\lambda_\infty = \frac{16}{3} n^2 \frac{\sigma T_r^3}{E} + \lambda_{SG}$$

λ_{SG} here denotes the solid and/or gas conductivity.

Anisotropic scattering is included by proper scaling of the optical thickness τ_0 and the albedo ω_0 [7].

Equation (8) has been derived for a gray medium. If the spectral variation of the effective extinction cross section and albedo is not too large, the parameters τ_0 and ω_0 can be interpreted as the spectrally averaged values. This gray solution closely fits experimental results for the loss coefficient k of organic fiber mats in air for different mean temperatures, fiber densities, boundary emissivities, and thicknesses [7].

As an example, measurements are presented for a low-density fiber mat ($\rho = 7\ \mathrm{kg \cdot m^{-3}}$, thickness $d = 39$ mm, fiber diameter $\phi \approx 40\ \mu m$) with low emissivity boundaries and where the gas pressure p_{GAS} was varied from high vacuum to ambient pressure (Fig. 5). At gas pressures below 10^{-1} Pa gas conduction is negligibly small. As contributions from solid conduction via the fiber mat are also negligible, the thermal transport under these

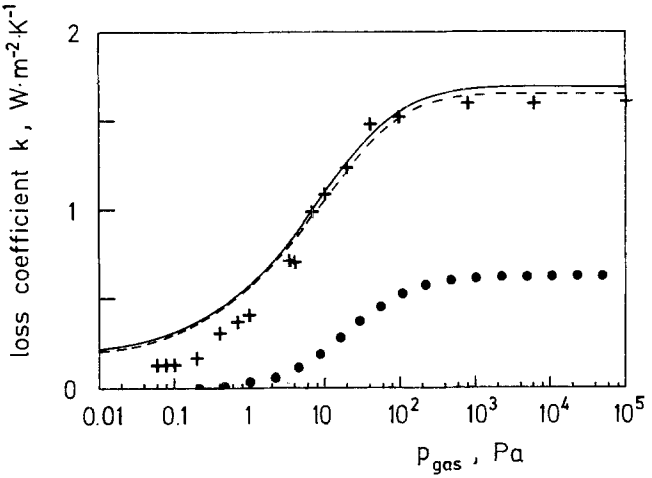

Fig. 5. Thermal loss coefficient k for a low-density organic fiber mat as a function of gas pressure p_{gas} for $T = 305$ K, $d = 0.039$ m, $\varepsilon = 0.05$, $\rho \approx 7.1\ \mathrm{kg \cdot m^{-3}}$: (+) experiment; (——) calculation with Eqs. (8) and (9); (– – –) five-flux solution; $(\cdots)\, k_{gas} = \lambda_{gas}/d$ with λ_{gas} from Eq. (9).

conditions is governed by IR radiation. The low emissivity ($\varepsilon \approx 0.05$) of the aluminium foil boundary is responsible for the small loss coefficient $k \approx k_{rad} \approx 0.1\ \mathrm{W \cdot m^{-2} \cdot K^{-1}}$.

For N_2 pressure above 100 Pa gas conduction is fully developed. For $\lambda_{GAS} \approx 0.026\ \mathrm{W \cdot m^{-1} \cdot K^{-1}}$ and $d = 0.039$ m, $k_{GAS} \approx 0.65\ \mathrm{W \cdot m^{-2} \cdot K^{-1}}$ is calculated. The measured loss coefficient in this pressure range is $k \approx 1.6\ \mathrm{W \cdot m^{-2} \cdot K^{-1}}$ and thus considerably larger than expected from an additive superposition of the conductive (k_{GAS}) and the radiative (k_{rad}) contribution:

$$k > k_{rad} + k_{GAS} = (0.1 + 0.65)\ \mathrm{W \cdot m^{-2} \cdot K^{-1}} = 0.75\ \mathrm{W \cdot m^{-2} \cdot K^{-1}}$$

This phenomenon can be explained by the assumption that there is a radiative boundary layer in front of the low-emissivity foil [20]. Within such a layer an enhanced temperature gradient will increase significantly the heat conduction into or out of the low-density insulation system. Further inside the fiber mat heat is transported by conduction and radiation.

Equation (8) can be used to model the complex interaction of gas conduction and radiation. The gas conduction λ_{gas} is obtained from

$$\lambda_{gas} = \frac{\lambda_{gas,0}}{1 + (\mathrm{const}/p_{gas})} \tag{9}$$

where $\lambda_{gas,0} = 26 \cdot 10^{-3}\ W \cdot m^{-1} \cdot K^{-1}$. We used the same fiber optical data as found in Ref. 7, i.e., albedo $\omega_0 = 0.54$, $e = 13.5\ m^2 \cdot kg^{-1}$, and density $\rho = 7.2\ kg \cdot m^{-3}$.

Experiment and calculated data are compared in Fig. 5. The best fit is obtained with const = 20 Pa. Further verification of the reliability of Eq. (8) can also be shown by performing a five-flux calculation. Both theoretical curves differ by less than 3%. Although the experimental data and the calculations agree well above 10 Pa, at low gas pressures the calculated loss coefficient is twice as high as the measured one. This may be caused by the discreteness of the fiber system (the average pore size is about 8 mm), which is not included in the basic continuous transfer models.

3.2. Silica Aerogels

Silica aerogel, a translucent highly porous insulating material [16], is another example. The IR transmission spectrum is shown in Fig. 2. The low absorption region between the wavelengths of 3 and 5 μm causes considerable leakage of IR radiation, especially at elevated temperatures. Consequently, the thermal losses vary strongly with the emissivity of the boundaries. In addition, the coupling between the radiation field and the heat flux caused by solid conduction must also be taken into account.

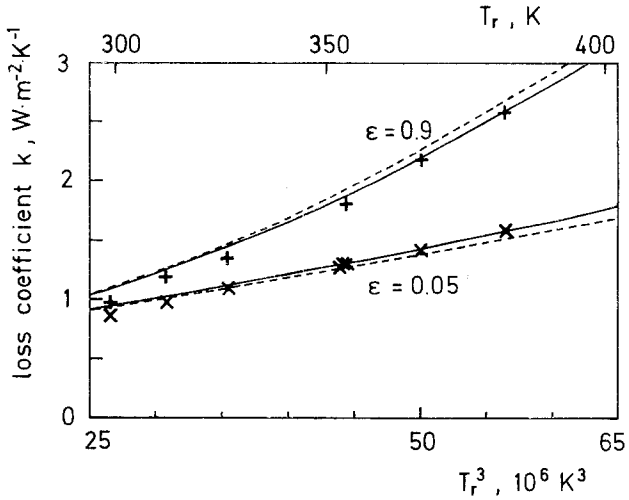

Fig. 6. Loss coefficient k of an aerogel tile ($\rho = 77\ kg \cdot m^{-3}$, $d = 9$ mm) as a function of mean temperature T_r: (+) x measurement; (——) numerical solution of general heat transfer equation; (---) appropriate spectral three-flux equation.

The heat transfer for combined radiation and conduction is described by an integrodifferential equation. It is very tedious to solve the exact equation numerically for a nongray medium such as aerogel, where the optical thickness $\tau_0(\Lambda)$ is a function of the wavelength. However, it was possible to generalize the approximate three-flux solution for gray media [Eq. (8)] to nongray media. Instead of the constant optical thickness τ_0, its spectral value $\tau_0(\Lambda)$ is used and Eq. (8) (with $\omega_0 = 0$) is integrated over the thermal spectrum with the Rosseland distribution $\partial e_\Lambda(T)/\partial e_b(T)$ as a weight factor [$e_\Lambda(T)$ being the spectral and $e_b(T) = \sigma T^4$ the total blackbody emissive power].

In Fig. 6 the loss coefficient of an aerogel tile ($\rho = 77\,\mathrm{kg \cdot m^{-3}}$ and $d = 9$ mm, boundary emissivities $\varepsilon = 0.05$ and 0.9) is compared to numerical solutions of the general integrodifferential equation and to the simple three-flux approach described above [13]. A solid conductivity $\lambda_s = 5.5 \cdot 10^{-3}\,\mathrm{W \cdot m^{-1} \cdot K^{-1}}$ used as input in both methods is most consistent with the experimental data. It should be noticed, however, that the spectral generalization of the three-flux equation is only an approximation and ought to be used with care.

4. CONCLUSION

The thermal transport in optically thick and optically thin insulations is now sufficiently well understood to allow data interpretation and optimization of insulating systems with respect to radiative transport and solid and gas conduction. However, some discrepancies between experiment and theory are still large enough to encourage future research.

ACKNOWLEDGMENT

This work was supported by the German Bundesministerium für Forschung und Technologie (BMFT).

REFERENCES

1. M. G. Kaganer, *Thermal Insulation in Cryogenic Engineering* (Israel Program for Scientific Translations, Jerusalem, 1969).
2. See, e.g., D. W. Yarbrough, R. S. Graves, F. J. Weaver, and D. L. McElroy, *ORNL/CON-215* (Oak Ridge National Laboratory, Oak Ridge Tenn., 1986).
3. D. Büttner, G. Löffler, R. Caps, and J. Fricke, *High Temp. High Press.* **18**:537 (1986).
4. J. Fricke, D. Büttner, R. Caps, J. Groß, and O. Nilsson, Loaded Fibrous Insulations—The Solid Conductivity, ASTM C16 Symposium, Bal Harbor, Fla. (Dec. 1987).
5. D. Büttner, J. Fricke, R. Krapf, and H. Reiss, *High Temp. High Press.* **15**:133 (1983).

6. J. Fricke, R. Caps, D. Büttner, U. Heinemann, E. Hümmer, and A. Kadur, *Solar Energy Mater.* **16**:267 (1987).
7. J. Fricke, R. Caps, E. Hümmer, G. Döll, M. C. Arduini, and F. DePonte, Optically Thin Fibrous Insulations, ASTM C16 Meeting, Bal Harbor, Fla. (Dec. 1987).
8. D. Büttner, J. Fricke, and H. Reiss, Analysis of Radiative and Solid Conducting Components of the Total Thermal Conductivity of an Evacuated Glass Fiber Insulation; Measurements with a $(700 \cdot 700)$ mm^2 Variable Load Guarded Hot Plate Device, AIAA 20th Thermophys. Conf., Williamsburg, Va. (June 1985).
9. R. Caps, *Strahlungswärmeströme in evakuierten thermischen Superisolationen*, Ph.D. Thesis (Physikalisches Institut der Universität Würzburg, Würzburg, 1985), Report E12-1285-1.
10. K.-G. Degen, *Wärmeleitfähigkeit von Kieselgur-Pulverisolationen*, Diplom. thesis (Physikalisches Institut der Universität Würzburg, Würzburg, 1988), Report E21-0488-1.
11. D. Büttner, J. Fricke, and H. Reiss, Analysis of Radiative and Solid Conduction Components of an Evacuated Glass Fiber Insulation, AIAA 20th Thermophys. Conf., Williamsburg, Va. (June 1985).
12. Y. S. Touloukian (ed.), *Thermal Conductivity, Nonmetallic Solids, Thermophysical Properties of Matter* (IFI/Plenum, New York, 1970).
13. G. Döll, *Wärmetransport durch optisch dünne, nichtgraue Medien*, Diplom. thesis (Physikalisches Institut der Universität Würzburg, Würzburg, 1987), Report E12-0987-3.
14. H. C. Hottel, A. F. Sarofim, W. H. Balzell, and I. A. Vasalos, *AIAA J.* **9**:1895 (1971).
15. J. Frickè, D. Büttner, R. Caps, G. Döll, E. Hümmer, A. Kreh, and H. Reiss, Load-Bearing Evacuated Fibrous Superinsulation, Improvements with Peg-Support and Metal-Coated Fibers, 20th Int. Therm. Conduct. Conf. Blacksburg, Va. (Oct. 1987).
16. J. Fricke, R. Caps, D. Büttner, U. Heinemann, E. Hümmer, and A. Kadur, Solar Energy Mater. **16**:267 (1987).
17. R. Caps and J. Fricke, in *Aerogels*, Springer Proceedings in Physics 6, J. Fricke, ed. (Springer Verlag, Heidelberg, 1986), p. 110 ff.
18. N. L. McKay, T. Timusk, and B. Farnworth, *J. Appl. Phys.* **55**:4064 (1984).
19. M. G. Kaganer, *Optika Spektrosk.* **26**:443 (1969).
20. P. Scheuerpflug, R. Caps, D. Büttner, and J. Fricke, *Int. J. Heat Mass Transfer* **28**:2299 (1985).

Printed in Belgium